ARMY RESEARCH LABORATORY

An Energy Budget Model to Calculate the Low Atmosphere Profiles of Effective Sound Speed at Night

by Arnold Tunick

ARL-MR-563 **May 2003**

NOTICES

Disclaimers

The findings in this report are not to be construed as an official Department of the Army position unless so designated by other authorized documents.

Citation of manufacturer's or trade names does not constitute an official endorsement or approval of the use thereof.

Destroy this report when it is no longer needed. Do not return it to the originator.

Army Research Laboratory
Adelphi, MD 20783-1197

ARL-MR-563 **May 2003**

An Energy Budget Model to Calculate the Low Atmosphere Profiles of Effective Sound Speed at Night

Arnold Tunick
Computational and Information Science Directorate, ARL

REPORT DOCUMENTATION PAGE

Form Approved
OMB No. 0704-0188

1. REPORT DATE *(DD-MM-YYYY)*	2. REPORT TYPE	3. DATES COVERED (From - To)
May 2003	Final	January 2003 to March 2003

4. TITLE AND SUBTITLE
An Energy Budget Model to Calculate the Low Atmosphere Profiles of Effective Sound Speed at Night

5a. CONTRACT NUMBER

5b. GRANT NUMBER

5c. PROGRAM ELEMENT NUMBER
62784A

6. AUTHOR(S)
Arnold Tunick

5d. PROJECT NUMBER

5e. TASK NUMBER

5f. WORK UNIT NUMBER

7. PERFORMING ORGANIZATION NAME(S) AND ADDRESS(ES)
U.S. Army Research Laboratory
ATTN: AMSRL-CI-EE
2800 Powder Mill Road
Adelphi, MD 20783-1197

8. PERFORMING ORGANIZATION REPORT NUMBER
ARL-MR-563

9. SPONSORING/MONITORING AGENCY NAME(S) AND ADDRESS(ES)
U.S. Army Research Laboratory
2800 Powder Mill Road
Adelphi, MD 20783-1197

10. SPONSOR/MONITOR'S ACRONYM(S)

11. SPONSOR/MONITOR'S REPORT NUMBER(S)

12. DISTRIBUTION/AVAILABILITY STATEMENT
Approved for public release; distribution unlimited.

13. SUPPLEMENTARY NOTES

14. ABSTRACT
This report presents an alternate energy budget model to the one implemented in the Acoustic Battlefield Aid (ABFA) for generating low atmosphere profiles of effective sound speed at night. The alternate model is based on the solution of a quartic equation for surface temperature, which assumes a balance between the net (long wave) radiative flux and the turbulent fluxes of heat and moisture close to the ground. In contrast, the model in ABFA assumes that the net surface radiation is constant with time at night, reduced only in the presence of clouds, and is balanced entirely by the surface heat flux. Therefore, the alternate model may be an improved calculation for this application.
However, some difficulties were encountered in the application of traditional Monin-Obukhov (M-O) profile theory for calculating nighttime turbulence structure from wind speed, temperature, and humidity difference data. Model breakdowns were problematic for a nighttime case when surface wind speeds were low, $U < 4.0\ ms^{-1}$, and skies were clear. During such stable and very stable conditions, the M-O scaling length too often became small—small enough to cause a computational sensitivity. Thus, we recommend that the alternate model in its present form be applied only when surface wind speeds and surface roughness lengths (i.e., canopy heights) can affect values for the M-O scaling length larger than about *13 m.*

15. SUBJECT TERMS
Surface layer, Monin-Obukhov similarity, computer model, CASES-99, WSCAFFIP, and acoustic attenuation

16. SECURITY CLASSIFICATION OF:			17. LIMITATION OF ABSTRACT	18. NUMBER OF PAGES	19a. NAME OF RESPONSIBLE PERSON
a. REPORT	b. ABSTRACT	c. THIS PAGE			Arnold Tunick
Unclassified	Unclassified	Unclassified	UL	30	19b. TELEPHONE NUMBER (*Include area code*) 301-394-1765

Standard Form 298 (Rev. 8/98)
Prescribed by ANSI Std. Z39.18

Contents

List of Figures

List of Tables

Acknowledgments

The author would like to thank Ron Meyers and Mike Mungiole of the U.S. Army Research Laboratory for offering helpful comments on this work.

1. Introduction

Advanced sensors and computer models for the surveillance, detection, identification, and tracking of sound-emitting targets in combat are rapidly emerging (*1,2*). Most new Army acoustic systems use unattended microphone sensors to construct small ground-based, beam-forming arrays to determine line-of-bearing angles, e.g., the remote netted acoustic detection system (*3*). At the same time, point-to-point transmission of acoustic signals is greatly influenced by variations in the wind flow, temperature field, and turbulence over varying topography and surface energy budgets (*4-6*). Thus, the Army is looking to implement the best possible acoustic propagation models, particularly those that will incorporate the impacts of the environment (e.g., the atmosphere, turbulence, and terrain) on acoustic signatures.

A key element in determining point-to-point acoustic transmission is modeling the variation of the effective speed of sound through the lower atmosphere. The effective speed of sound (c_{eff}), which accounts for the bearing of the sound source from a given receiver and the compass bearing of the mean wind, is readily derived from measured or modeled estimates of air temperature, relative humidity, and wind velocity. It is useful to define the effective speed of sound (c_{eff}) from the following expression given by Noble (*7*) and Osteshev (*5*):

$$c_{eff} = c_o + \overline{u}\cos(\theta_w - \pi - \theta_R) \quad , \tag{1}$$

in which $c_o = \sqrt{\frac{\gamma_s RT}{M}}$, $R = 8314.32\ J\,mol^{-1}K^{-1}$ is the universal gas constant, T is air temperature in Kelvin, M is molecular mass, $\gamma_s = \frac{c_p}{c_v}$ is the ratio of specific heats, $\overline{u}$ is the mean of the horizontal wind, θ_w is the bearing of the wind from North, θ_R is the bearing of the receiver from the source, and $\overline{u}\ \cos(\theta_w - \pi - \theta_R)$ is the component of the sound speed along the direction of propagation from the source to the receiver. As discussed in Osteshev (*5*), the effective sound speed in equation 1 is valid only for nearly horizontal propagation angles (*8*). In addition, Wong and Embleton (*9*) have deduced the ratio of specific heats and molar mass $\left(\frac{\gamma_s}{M}\right)$ as a function of temperature and humidity in the following form:

$$\frac{\gamma_s}{M} = 0.04833 + (R_h - 0.023)A_t \quad , \tag{2}$$

in which $A_t = 9.2 \times 10^{-5} + 5.5 \times 10^{-6}\, t + 4.25 \times 10^{-7}\, t^2$, R_h, is relative humidity (in the range 0.0 to 1.0), and t is air temperature (°C). Then, for applications in outdoor acoustics, sound speed differences across vertical layers will generally cause acoustic waves to be refracted upward if the effective sound speed decreases with height, and they will be refracted downward if sound speed increases with height.

Monin-Obukhov (M-O) similarity models (*10–14*) have been very well suited for such acoustic applications. For example, the energy budget and meteorological models implemented in the Acoustic Battlefield Aid (ABFA) (*15,16*) are relatively simple and quite robust for generating low atmosphere profiles of effective sound speed, especially for daytime convective atmospheres. However, for the nighttime case, the model in ABFA assumes that the net surface radiation is constant with time, reduced only in the presence of clouds, and is balanced entirely by the surface heat flux. Therefore, in this report, we are interested in testing the effectiveness (for this application) of an earlier quartic solution for the surface temperature (*17,18*), i.e., an alternate energy budget model, which explicitly computes the net (long wave) radiative flux and the turbulent fluxes of heat and moisture close to the ground. Then, the primary energy budget model results can be used to estimate profiles for wind speed, air temperature, and relative humidity, from which, effective sound speed information can be generated.[1]

2. Model Equations

2.1 A Quartic Solution for the Surface Temperature

The alternate surface energy budget model described in this section is a semi-empirical, equilibrium model (*17,18*) that explicitly computes each energy balance component, except the flux of energy into and out from the ground, which is computed simply as a percentage, 10% daytime and 5% nighttime, of the computed net radiation (*21*). The model's primary input are reference level (1 to 2 m) values for wind speed, air temperature, relative humidity, atmospheric pressure, surface thermal emissivity, soil water content, and cloud cover information. (For daytime calculations, the day of interest, longitude, and latitude of the site are required to determine the solar declination, hour, and zenith angles.) The model's primary output are calculations of the net radiation, the effective surface temperature, and the soil, sensible, and latent heat fluxes.

In accordance with Carson (*22*), it is assumed that the energy budget close to the ground (as shown in Figure 1) can be written as

$$R_{net} = H + L'E + G \quad , \tag{1}$$

in which R_{net} is the net radiative flux, H is the turbulent sensible heat flux, $L'E$ is the latent heat flux attributable to surface evaporation, and G is the flux of heat into or out of the soil. Positive values of R_{net} and G are chosen to represent fluxes directed downward while positive H and $L'E$ values represent fluxes directed away from the air-soil interface.

[1]Note that Swanson and Reichard (*19*) and Swanson (*20*) have also reported on the use of M-O similarity-type formulations to generate low atmosphere sound speed profiles. However, they based their estimates of the M-O scaling constants on data retrieved from a ground-based micrometeorological instrument rather than from energy budget principles, as discussed in this report. Nevertheless, their goal was very similar, i.e., to incorporate similarity-based estimates of effective sound speed within probability of detection (sensor performance) algorithms for unattended acoustic sensor arrays.

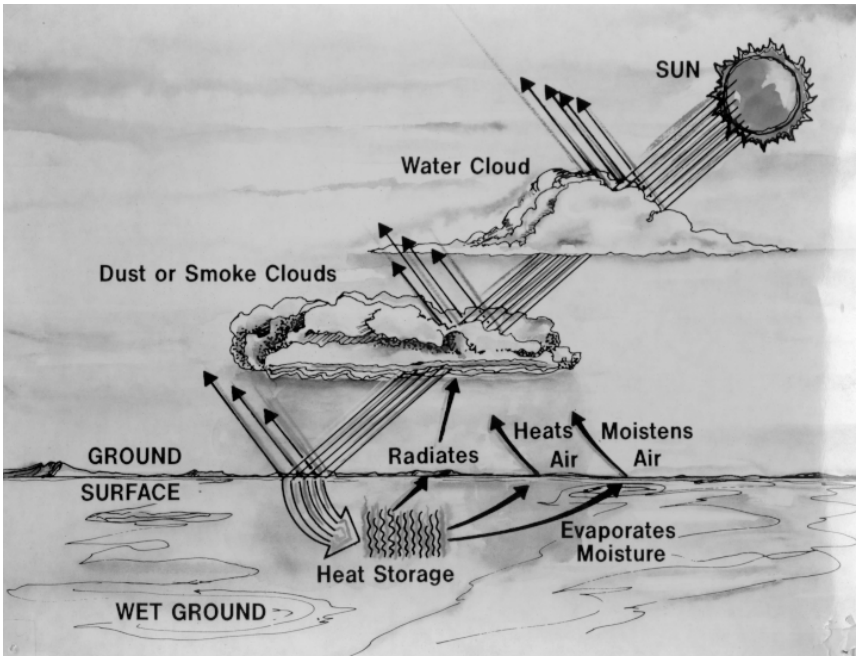

Figure 1. The radiation and energy budget close to the ground (illustrated by F.V. Hansen, 1993).

The formulations in the model used to compute the incoming short wave solar radiation ($R_{S\downarrow}$) for daytime cloudless skies are patterned after Meyers and Dale (*23*) and are augmented as needed with empirical results by Haurwitz (*24*) to account for cloudy skies, i.e.,

$$R_{S\downarrow} = I = I_o T_R T_P T_W T_A \cos Z \quad , \tag{2}$$

in which I_o is the extra-terrestrial flux density at the top of the atmosphere on a surface normal to the incident radiation, Z is the solar zenith angle, and T_i are the transmission coefficients for Rayleigh scattering (R), absorption by permanent gases (P), water vapor (W), and absorption and scattering of aerosols (A). The empirically derived transmission coefficient for cloudy skies (*24*) is defined by the ratio of insolation with partly or completely covered sky to insolation of cloudless skies.

Gates (*25*) gives the expression for downward long wave radiation ($R_{L\downarrow}$) for clear skies in the model, i.e.,

$$R_{L\downarrow} = -170.9 + 1.195\,\sigma\, T_r^4 \quad , \tag{3}$$

in which $R_{L\downarrow}$ is in watts per meter^2, $\sigma = 5.6697 \times 10^{-8}$ W m^{-2} K^{-4}, and T_r the reference level (1 to 2 m) temperature in Kelvin. From Paltridge and Platt (*26*) an addition to equation 3 is made to account for clouds, giving the total expression as

$$R_{L\downarrow} = -170.9 + 1.194\,\sigma\, T_r^4 + 0.3\,\varepsilon_c\,\sigma\, T_c^4 (cc) \quad , \tag{4}$$

in which ε_c is the long wave flux emissivity of the cloud base, T_c is the temperature of the cloud base in Kelvin, and cc is the fractional cloud cover. Having an estimate of the cloud height, one can approximate T_c, assuming an average of the dry and moist adiabatic lapse rate.

The upward long wave radiative flux ($R_{L\uparrow}$) is computed by a formulation from Yamada (*27*), i.e.,

$$R_{L\uparrow} = \varepsilon \sigma T_g^4 + (1 - \varepsilon) R_{L\downarrow} \quad , \tag{5}$$

To evaluate equation 5, one requires an estimate of the effective ground or surface temperature, T_g. We achieve this through the application of M-O similarity formulations (*10–14*) and the flux-gradient hypothesis as advocated by Dyer (*12*) and Webb (*14*).

The similarity-based expressions for the sensible and latent heat fluxes are defined by the MARIAH algorithm (*28*) and are expressed as

$$H = -c_p \rho u_* \theta_* = -\frac{c_p \rho k^2 V_r (T_r - T_g)}{\phi_m \phi_h \ln\frac{z-d}{z_0} \ln\frac{z-d}{z_h}} \tag{6}$$

and

$$L'E = -L' \rho u_* q_* = -\frac{L' \rho k^2 V_r (q_r - q_g)}{\phi_m \phi_q \ln\frac{z-d}{z_0} \ln\frac{z-d}{z_h}} \quad , \tag{7}$$

in which c_p is specific heat; ρ is air density; k is von Karman's constant; V_r is the reference height wind speed; L' is the latent heat of vaporization; q_r and q_g are the reference height and effective surface values for specific humidity, respectively; u_* is the friction velocity (m/s); θ_* is the potential temperature scaling constant (K); q_* is the specific humidity scaling constant (kg/kg); z is height above ground in meters; d is displacement height in meters (~70% of the principal roughness element); z_0 is the aerodynamic (surface) roughness height in meters (~14% of the principal roughness element); z_h is the thermal roughness height in meters (~13% of the aerodynamic roughness); and ϕ_m, ϕ_h, and ϕ_q are the dimensionless wind shear, dimensionless temperature lapse rate, and dimensionless humidity lapse rate, respectively. Here, the dimensionless term for humidity is assumed to be equal to the dimensionless temperature lapse, i.e., $\phi_q = \phi_h$, even though field observations have shown that this is not always correct. Also, for stable and very stable conditions at night, Mahrt (*29*) recommends setting $z_0 = z_h$. Equations 6 and 7 can be evaluated in a straightforward manner, given expressions for the dimensionless shear and lapse rate terms.

Following the recommendations of Högström (*30*), we use

$$\phi_m = [1 - 19(z/L)]^{-1/4} \text{ and } \phi_h = 0.95[1 - 11.6(z/L)]^{-1/2} \quad , \tag{8}$$

for daytime unstable atmospheric conditions, and we use

$$\phi_m = 1 + 5.3(z/L) \text{ and } \phi_h = 1 + 8(z/L) \tag{9}$$

for nighttime stable atmospheric conditions[2], where Busch (*11*) defines the M-O scaling ratio as

$$\frac{z}{L} = k\frac{g}{\theta_v}\frac{\theta_{v*}}{u_*^2}z \quad , \tag{10}$$

in which $\theta_v = T_r(1 + 0.61q_r)$ is the virtual potential temperature and $\theta_{v*} = \theta_* + 0.61T_r q_*$ is the virtual potential temperature scaling constant (q_* is the specific humidity scaling constant). Here, reference level specific humidity, q_r, is determined as a function of relative humidity (R_h), atmospheric pressure (P_r), and air temperature (T_r) with the formulation from Rogers (*31*), i.e.,

$$q_r = \frac{3.8R_h}{P_r}\exp\left(5.44\times10^3\left(\frac{1}{2.73.15} - \frac{1}{T_r}\right)\right) \quad . \tag{11}$$

In contrast, surface specific humidity, q_g, is determined as a function of the following parameters (*32*): reference level specific humidity (q_r), saturation specific humidity at the surface (q_s) (i.e., substitute into equation 11 $R_h = 100\%$ and $T_r = T_g$), the water capacity of the field (θ_f), and finally, soil water content (w_s). As a result, surface specific humidity can be expressed as

$$q_g = (1-\delta)\ q_r\ + \delta\ q_s \quad , \tag{12}$$

in which

$$\delta = 0.25\left(1 - \cos\left(\frac{\pi\ w_s}{\theta_f}\right)\right)^2 \qquad \text{for } w_s < \theta_f \tag{13}$$

$$\text{and} \qquad \delta = 1 \qquad \text{for } w_s > \theta_f \ .$$

Next, we substitute equations 6 and 7 for H and $L'E$ into equation 1 and define the soil heat flux (G) as $G = \beta R_{net}$ (where $R_{net} = R_{L\downarrow} - R_{L\uparrow} + R_{S\downarrow} - R_{S\uparrow}$ and $R_{S\uparrow} = \alpha R_{S\downarrow}$). Then after some rearranging, we solve equation 1 for T_g, which gives the quartic form for the equilibrium model as

$$\begin{aligned}(1-\beta)\left(\varepsilon\,\sigma\,T_g^4 - (1-\alpha)R_{S\downarrow} - \varepsilon\,R_{L\downarrow}\right) + T_g\left(\frac{c_p\ \rho\ k^2\ V_r}{\phi_m\ \phi_h\ \ln\frac{z-d}{z_o}\ \ln\frac{z-d}{z_h}}\right) \\ -\frac{c_p\ \rho\ k^2\ V_r\ T_r}{\phi_m\ \phi_h\ \ln\frac{z-d}{z_o}\ \ln\frac{z-d}{z_h}} - \frac{L'\ \rho\ k^2\ V_r\ (q_r - q_g)}{\phi_m\ \phi_h\ \ln\frac{z-d}{z_o}\ \ln\frac{z-d}{z_h}} = 0\end{aligned} \tag{14}$$

in which α is the surface short wave reflectivity, commonly called "albedo," and β is the percentage (e.g., 10% daytime and 5% nighttime) of the computed net radiation used to calculate the soil (ground storage) heat flux. Naturally, at night, $R_{S\downarrow} = 0$. The quartic equation is resolved numerically via a Newton-Raphson iterative scheme.

[2]Alternately, Webb (*14*) suggests $\phi_m = \phi_h = 1 + 5(z/L)$ for nighttime stable conditions.

2.2 The Energy Budget Model Implemented in ABFA

Wilson (*15*) and Wilson and Szeto (*16*) report on the development of the prototype model ABFA for the analysis of atmospheric refraction and turbulence effects on acoustical detection and tracking systems. Among the meteorological input capabilities embedded in ABFA is a surface energy budget model for generating low atmosphere profiles of effective sound speed. The ABFA energy budget model is based on the empirical formulations of Burridge and Gadd (*33*), as discussed in Stull's (*21*) textbook (Chapter 7). For the nighttime case, the net long wave radiation is given by the following expression:

$$R_L\uparrow - R_L\downarrow = \left(0.08\rho c_p\right)\left(1.0 - 0.1\sigma_H - 0.3\sigma_M - 0.6\sigma_L\right) \quad , \tag{15}$$

in which σ_H, σ_M, and σ_L are the cloud cover fractions for high, middle, and low clouds, respectively. (In contrast, cloud cover is accounted for in the parameterization for $R_L\downarrow$ shown in equation 4.) Clearly, this is a much simpler formulation than the solution of the quartic.

In ABFA, the net surface radiation is balanced entirely by the surface heat flux, Q, so that the M-O temperature scaling constant is calculated as

$$\theta_* = -\frac{Q}{\rho c_p u_*} \quad , \tag{16}$$

and the M-O scaling length is derived as

$$L = -\frac{u_*^3}{k\dfrac{g}{\theta}\dfrac{Q}{\rho c_p}} \quad , \tag{17}$$

where the friction velocity can be determined from the reference height wind speed (Vr) and values for roughness length (z_0) and displacement (d), i.e.,

$$u_* = \frac{k V_r}{\phi_m \ln\left(\dfrac{z-d}{z_0}\right)} \quad . \tag{18}$$

Thus, the ABFA energy budget model output is used to estimate the similarity-based, log-linear profiles for wind speed and temperature extended upward through the surface layer, as discussed next.

2.3 The Similarity-Based Profiles

Given values for the M-O scaling constants from energy budget considerations, the formulations of Benoit (*34*) and Nickerson and Smiley (*35*) are applied to determine the similarity-based profiles for wind velocity, temperature, and specific humidity as follows:

$$V(z) = V_r + \frac{u_*}{k}\left[\ln\left(\frac{z}{z_r}\right) - \psi_m\left(\frac{z}{L}\right) + \psi_m\left(\frac{z_r}{L}\right)\right] \quad , \tag{19}$$

$$T(z) = T_r + \frac{\theta_*}{k}\left[\ln\left(\frac{z}{z_r}\right) - \psi_h\left(\frac{z}{L}\right) + \psi_h\left(\frac{z_r}{L}\right)\right] , \quad (20)$$

and

$$q(z) = q_r + \frac{q_*}{k}\left[\ln\left(\frac{z}{z_r}\right) - \psi_q\left(\frac{z}{L}\right) + \psi_q\left(\frac{z_r}{L}\right)\right] , \quad (21)$$

where, for the nighttime case, the diabatic influence functions for momentum and heat, ψ_m and ψ_h respectively, are given by Webb (*14*), i.e.,

$$\psi_m = \psi_h = -5\frac{z}{L} \quad . \quad (22)$$

Here, we assume that $\psi_q = \psi_h$.

For extended profiles of relative humidity, we use equation 11 and the following expression for atmospheric pressure given by Campbell and Norman (*36*), i.e.,

$$P(z) = P_r \exp\left(\frac{-(z - z_r)}{8200.}\right) \quad (23)$$

which yields

$$R_h(z) = 100.0\frac{q(z)P(z)}{3.8}\exp\left(5.44\times10^3\left(\frac{1}{273.15} - \frac{1}{T(z)}\right)\right)^{-1} \quad . \quad (24)$$

3. Model Results

3.1 A Hypothetical Case

A hypothetical nighttime case is outlined in Table 1. Input parameter values were chosen to represent low wind speeds and cool temperatures over a relatively smooth surface. For this example, the primary output parameters from the alternate energy budget model (described previously) are given in Table 2. First, it is shown that fairly good closure exists for this calculation, i.e., $R_{net} - G$ is approximately equal to $H + L'E$. This result helps to validate the model for partitioning the net radiation into its surface flux components. The small error (i.e., $\Delta = 6.83\ Wm^{-2}$) may be attributed to the approximation for soil heat flux. Second, the estimate for surface temperature, i.e., $T_g = T_r - 2.25$ K, appears to be quite reasonable for moderately stable conditions (i.e., $L = 35$ m). Third, the M-O scaling constants appear to be valid and useful, so that applying equations 19 through 24 provides the nighttime profiles for wind velocity, air temperature, and relative humidity for the layer $z \leq 60$ m (see Figure 2).

Table 1. Energy budget model parameters

Parameter	Symbol	Value
Reference atmospheric pressure	P_r	1000 mbar
Reference relative humidity	R_h	40 %
Reference air temperature	T_r	283.15 K
Reference wind velocity	V_r	3.0 ms^{-1}
Reference height above ground	z_r	2.0 m
Principal roughness element or canopy height	h	0.50 m
Surface (long wave) emissivity	ε	0.98
Soil water content	w_s	0.13 m^3m^{-3}

Table 2. Energy budget model results

Parameter	Symbol	Value
Net radiative flux	R_{net}	–86.62 Wm^{-2}
Soil (ground storage) heat flux	G	–4.33 Wm^{-2}
Sensible heat flux	H	–114.50 Wm^{-2}
Evaporative (latent) heat flux	$L'E$	+ 25.38 Wm^{-2}
Friction velocity	u_*	0.35 ms^{-1}
Temperature scaling constant	θ_*	0.27 ºK
Humidity scaling constant	q_*	–2.35E-05 $kgkg^{-1}$
Monin-Obukhov scaling length	L	34.64 m
Surface air temperature	T_g	280.90 ºK

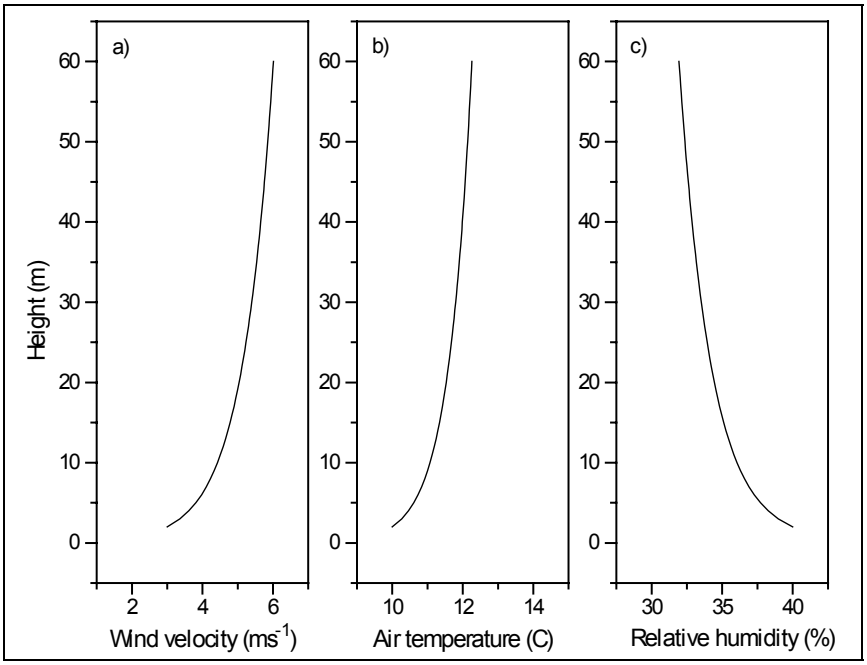

Figure 2. Typical similarity-based profiles for the nighttime case derived from the energy budget model: a) wind velocity (in units ms^{-1}), b) air temperature (in units C), and c) relative humidity (in percent).

Next, we apply equations 1 and 2 and the data shown before to derive the extended profiles for the effective speed of sound (see Figure 3). In Figure 3, the effective sound speed is determined for upwind propagation (left), i.e., the bearing of the receiver from the source and the direction of the wind from north are the same, and for downwind propagation (right), i.e., the bearing angles are 180º opposite. An asymmetry exists in the graph so that the profile for downwind propagation (on the right-hand side) is increasing with height above ground level, while the curve for upwind propagation (on the left side) is decreasing (slightly) with height. The effect that such profile variations in sound speed will have on short range acoustic attenuation is discussed next.

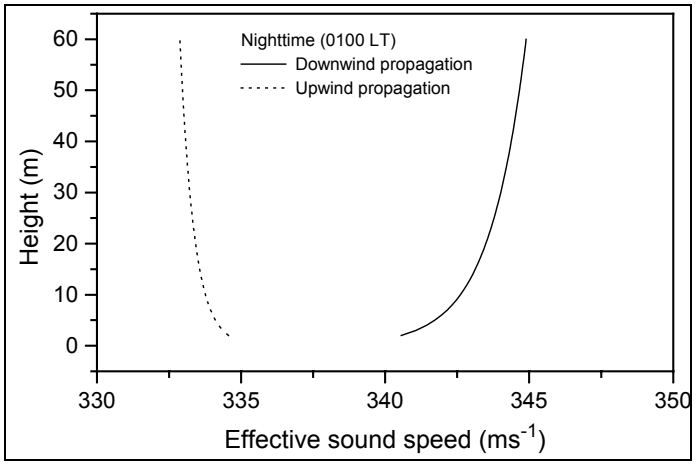

Figure 3. Low atmosphere profiles of the effective speed of sound derived from the energy budget model for upwind propagation (dashed) and downwind propagation (solid).

3.2 Approximation of Short Range Acoustic Attenuation

To briefly examine short range acoustic attenuation at night, we use the low atmosphere profiles of wind speed, temperature, and relative humidity (shown before) as input to a flat earth, non-turbulent acoustic propagation model called the Windows (version) Scanning Fast Field Program (WSCAFFIP). WSCAFFIP is a numerical code developed for assessing environmental effects on short range acoustic attenuation (*7,38*). WSCAFFIP determines acoustic attenuation as relative sound pressure loss with range and azimuth for a given frequency and source-to-receiver geometry. WSCAFFIP contains propagation algorithms to represent the effects of atmospheric refraction, diffraction, absorption, and reflection (ground impedance) on acoustic transmission. Table 3 lists the model parameters for an initial approximation of short range acoustic attenuation over an open grass-covered ($h = 0.5$ m) field. Figures 4 and 5 show the WSCAFFIP results corresponding to the modeled profiles of effective sound speed generated by the alternate (quartic) model.

Table 3. WSCAFFIP model parameters

Parameter	Symbol	Value
Distance of receiver from source	x	1000 m
Range resolution	Δx	10 m
Bearing of receiver from source	θ_R	90º
Bearing of the wind from North	θ_w	90º (upwind) and 270º (downwind)
Source height above ground	h_S	2 m
Receiver height above ground	h_R	1 m
Frequency of interest	f	100 - 1000 Hz
Ground porosity (tall grass pasture)	Ω_p	0.675
Flow resisitivity (tall grass pasture)	σ_r	330 kPa s m^{-2}

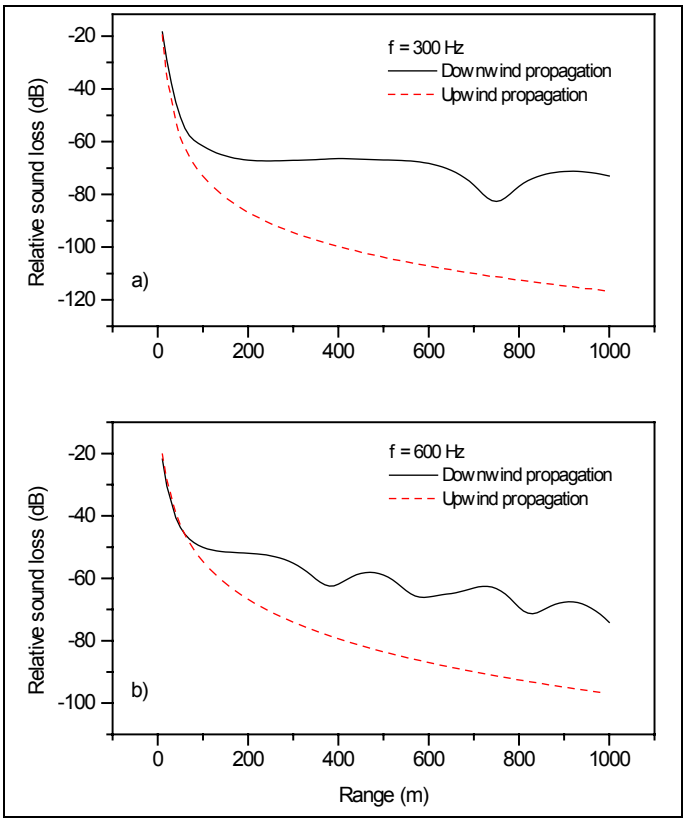

Figure 4. Line plots of acoustic attenuation versus range for upwind propagation (dashed) and downwind propagation (solid), (i.e., WSCAFFIP model results for 300 Hz and 600 Hz, only).

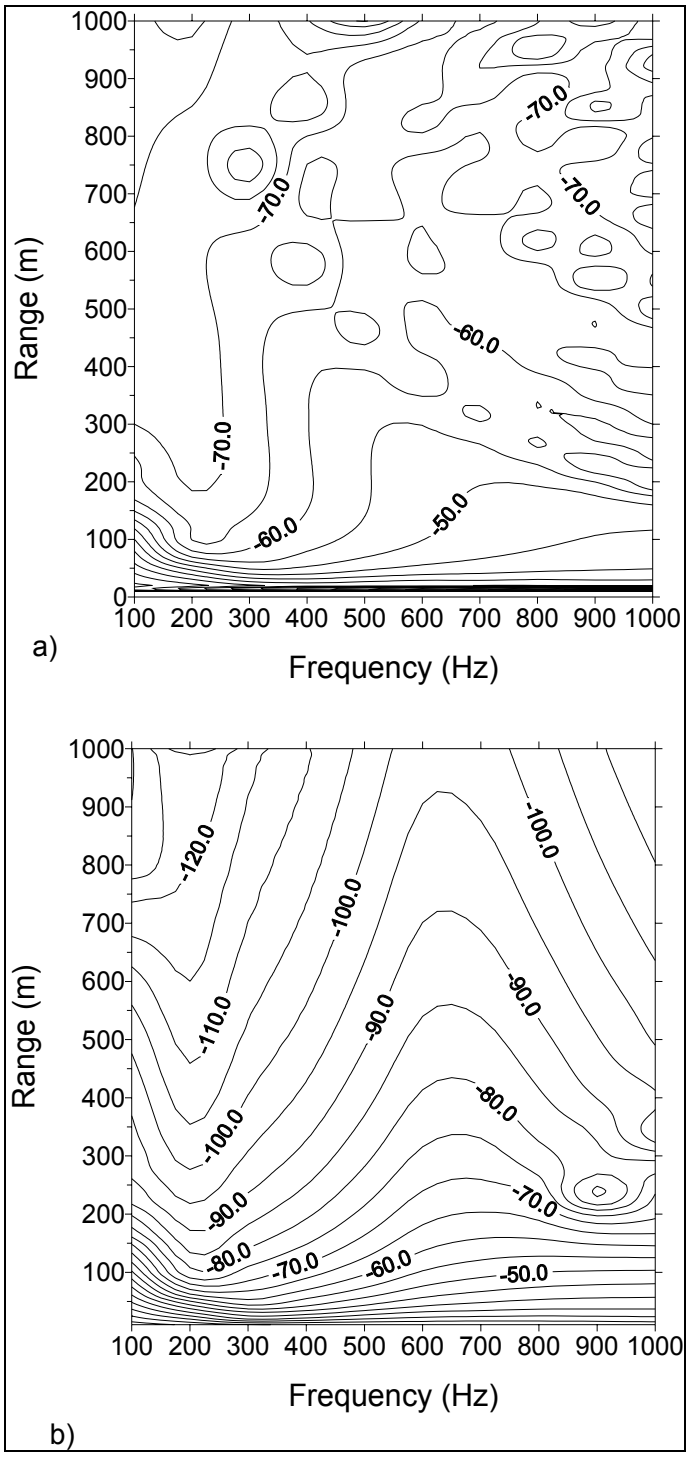

Figure 5. Contour graphs of acoustic attenuation as a function of frequency and range for downwind propagation (top) and upwind propagation (bottom) (i.e., WSCAFFIP model results for 100 Hz through 1000 Hz, inclusive).

As stated earlier, acoustic waves will tend to be refracted downward as the effective sound speed increases with height and refracted upward as the effective sound speed decreases with height. Therefore, one might expect the amounts of attenuation (in part) to depend on the strength of the sound speed profile gradient between the ground and the model top. Because generally, the effective sound speed profile for upwind propagation has values decreasing with height, we would expect to see greater attenuation with range at each frequency for upwind propagation as a result. The line plots of relative sound loss with range in Figure 4 (for 300 Hz and 600 Hz only) and the contour graphs of attenuation as a function of range and frequency shown in Figure 5 (for 100 to 1000 Hz inclusive) show this result satisfactorily.

In contrast, the behavior of the downwind propagation attenuation curves can be understood in terms of "ducting" of acoustic modes. For this example, the sound speed profile forms an acoustic duct between the surface and 60 m. At lower frequencies (100 to 200 Hz), acoustic waves may be too long for any significant ducting to occur. At 300 Hz, there appear to be one or two trapped modes, while at 400 Hz (and greater) several modes appear to be trapped, creating the interference pattern. In this way, ducting of acoustic energy across the lower boundary layer at night is greatly affected by local meteorological profile structure.

3.3 Comparison to Observations

At the start of this project, it was thought feasible to present modeled profiles of effective sound speed for the nighttime case in comparison to values of effective speed of sound derived from selected micro-meteorological data. As an example, the tower data used to generate the three time-height series shown in Figure 6 were collected as part of the 1999 Cooperative Atmosphere-Surface Exchange Study (CASES-99) (*39*). CASES-99 was an extensive field experiment that focused on the nocturnal boundary layer (NBL) under mainly clear sky, light near surface wind conditions (this included occurrences of weak and intermittent turbulence). The experimental period was from October 1 to 31, 1999. The test area for CASES-99 was near Leon, KS (50 km) east of Wichita, KS. The test site was chosen (in part) because of its relatively flat terrain (average slopes were 0.5 degree). A large number of instruments were deployed in an area 4.8×3.2 km. These instruments included a heavily instrumented 55-m tower, numerous 10-m towers, multiple radar, lidar, scintillometers, tethersondes, rawinsondes, and research aircraft (see http://www.joss.ucar.edu/cases99).

The subset of CASES-99 data shown in Figure 6 is from the first intensive observing period (IOP) on 5 October 1999 and includes the measurements of wind velocity, air temperature, relative humidity (5 min averaged) taken on the 55-m main tower approximately 5 km southeast of Leon, KS (latitude: 37 deg 38.88' N, longitude: 96 deg 44.14' W, elevation 433.7 m above sea level) in an open field of mostly dry grasses, approximately 0.15 m in height (on average). Surface roughness height for the site was determined to be about 2 cm and thermal emissivity was estimated at 0.98 (*40*).

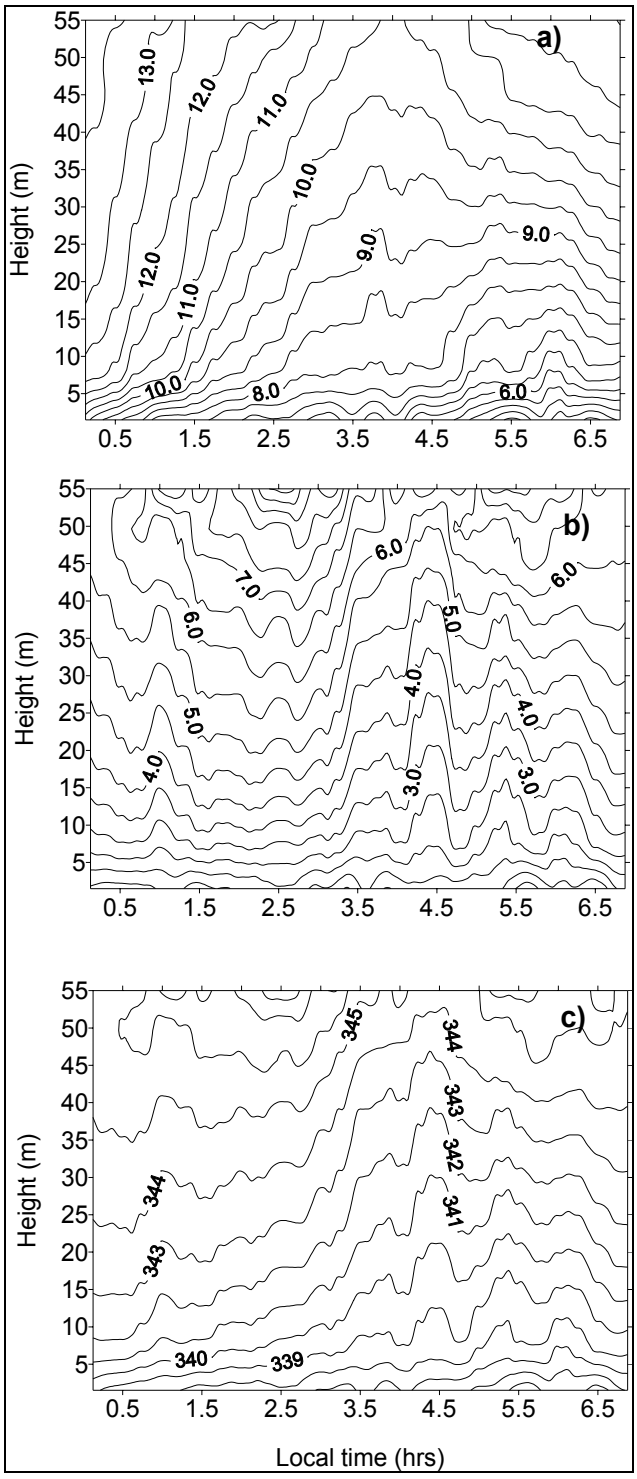

Figure 6. Time-height series of a) air temperature (in units C), b) mean horizontal wind speed (in units ms^{-1}), and c) effective sound speed (in units ms^{-1}), generated from CASES-99 (IOP-1) field data.

However, we experienced some difficulties in the application of traditional M-O profile theory for calculating nighttime turbulence structure from temperature, humidity, and wind speed difference data (see equations 6, 7, and 14). As an example, Figure 7 shows a time series of the modeled surface temperature (T_g), the 5-m measured temperature (T_r), and the 5-m measured wind speed (U_r) for the first nighttime IOP. For this example, reference height is $z_r = 5$ m and the canopy height is $h = 0.15$ m. Certainly, the surface temperature estimates are unrealistically low. This "runaway cooling," according to Mahrt (*29*), is a known defect in computer models that attempt to estimate meteorological gradients near the ground at night (during very stable conditions) with M-O similarity functions. To illustrate the problem further, Figure 8 shows a plot (at $t =$ 0.125 hr past midnight) of the estimated surface temperature (T_g), the estimated M-O scaling length (L), and the estimated dimensionless wind shear (ϕ_m) as a function of the 5-m reference height wind speed (U_r), as the wind speed is varied from $U_r = 1.0$ ms^{-1} to $U_r = 10.0$ ms^{-1}. In addition, the data in Table 4 and Figure 9 show a more detail view of the results plotted in Figure 8. The data clearly show that the model calculation collapses at $U_r = 3.6$ –3.8 ms^{-1}, where $T_g \leq 5.0$ *C*, $L \leq 8.0$ m, and $\phi_m \geq 1.6$. Then, for still lower wind speeds, L becomes very small—small enough to cause a computational sensitivity, as evidenced in the plot for ϕ_m. Given that both ϕ_m and ϕ_h are needed to define two principal components of the quartic, it can be reasoned that when L is small and the ϕ's are large, the model defaults to a kind of radiative equilibrium, where little heat energy (sensible, latent, or released from the soil) is available to offset the radiative term. When this occurs, i.e., when turbulence collapses, the model results are invalid.

As a final point, we consider the effect on the model results brought about by varied surface roughness (see Figure 10). Recall that for this example, the canopy height is *h=0.15* m (short grass) and the roughness length is $z_0 = 0.02$ m. In Figure 10, when $U_r = 3.6$ ms^{-1} and the canopy height < 0.25 m, the model again breaks down. Thus, for whatever the order of wind speed and roughness length, there appears be a derivable limit beyond which the calculation should be discounted. The arrow on Figure 9 suggests such a limit.

It is interesting to note that others had previously reported difficulties in the use of similarity-based models for the nighttime case (in the calculation of optical turbulence intensity [C_n^2]) (*41–43*). As an example, Figure 11 shows results from the *CN2* over-land optical turbulence model (*42,43*), derived from two levels (above ground) of conventional micro-meteorological information as input (i.e., wind speed, temperature, and humidity retrieved on farmland, over flat barren soil, under mostly clear skies). Although the *CN2* model estimates are in fairly good agreement with the observations during daytime hours, there are several instances at night when the model results show either a consistent bias (about a factor of 2 and mainly underestimated) in comparison to the measured turbulence data or the model results fluctuate toward extreme (minimum) values. Here, the largest errors occur when there is a computational sensitivity, as described before. Average surface layer wind speeds for the nighttime periods shown in Figure 11 were approximately 3 to 4 ms^{-1}.

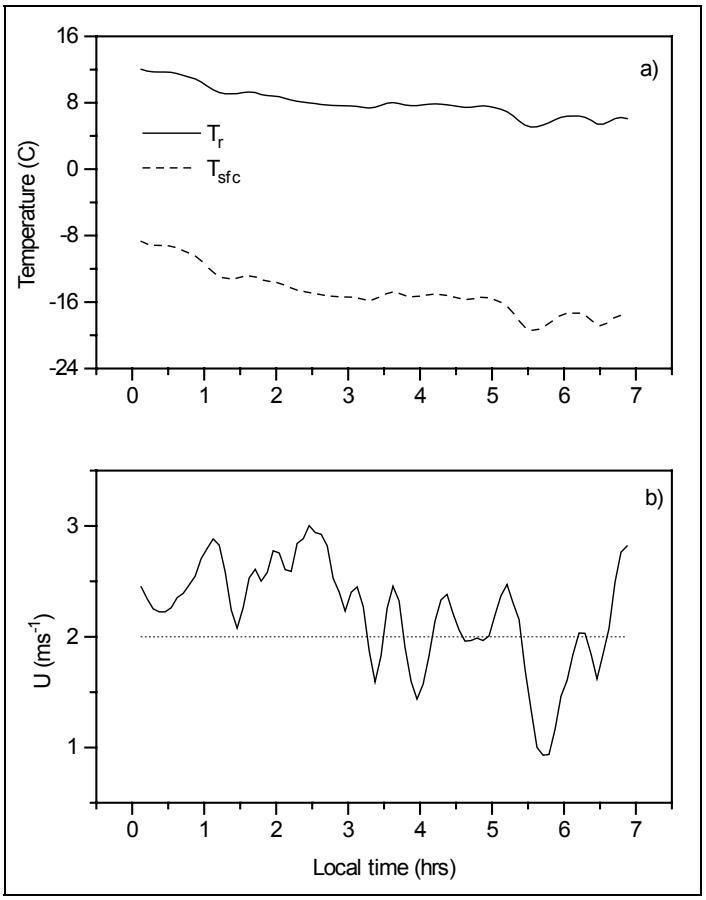

Figure 7. Time series of a) modeled surface temperature (T_g) and the 5-m temperature (T_r) and b) the 5-m measured wind speed (U_r) for the first nighttime IOP. (The dotted line in Figure 7b helps to show the large amount of data in this example where $U \leq 2.0\ ms^{-1}$.)

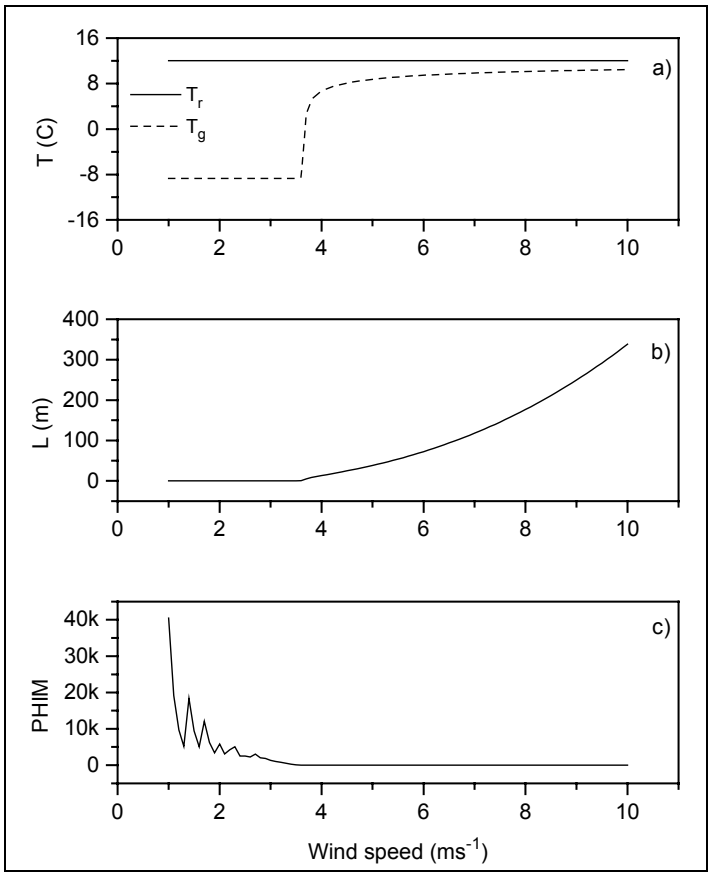

Figure 8. A plot at t = 0.125 hr of a) the estimated surface temperature (T_g), b) the estimated M-O scaling length (L), and c) the estimated dimensionless wind shear (ϕ_m) as a function of the 5-m reference height wind speed (U_r).

Table 4. Breakdown of M-O similarity models for the nighttime case

U_r **(ms^{-1})**	T_g **(C)**	L **(m)**	ϕ_m
3.2	–8.698	0.005	837.346
3.3	–8.698	0.008	547.225
3.4	–8.697	0.016	275.226
3.5	–8.682	0.066	71.424
3.6	***–8.447***	***0.275***	***18.173***
3.7	***2.579***	***4.914***	***1.964***
3.8	5.140	8.477	1.559
3.9	6.062	10.945	1.433
4.0	***6.647***	***13.245***	***1.358***
4.1	7.072	15.504	1.306
4.2	7.403	17.780	1.267
4.3	7.671	20.096	1.236
4.4	7.896	22.471	1.211
4.5	8.088	24.908	1.190
4.6	8.255	27.426	1.173
4.7	8.401	30.016	1.158
4.8	8.532	32.693	1.145

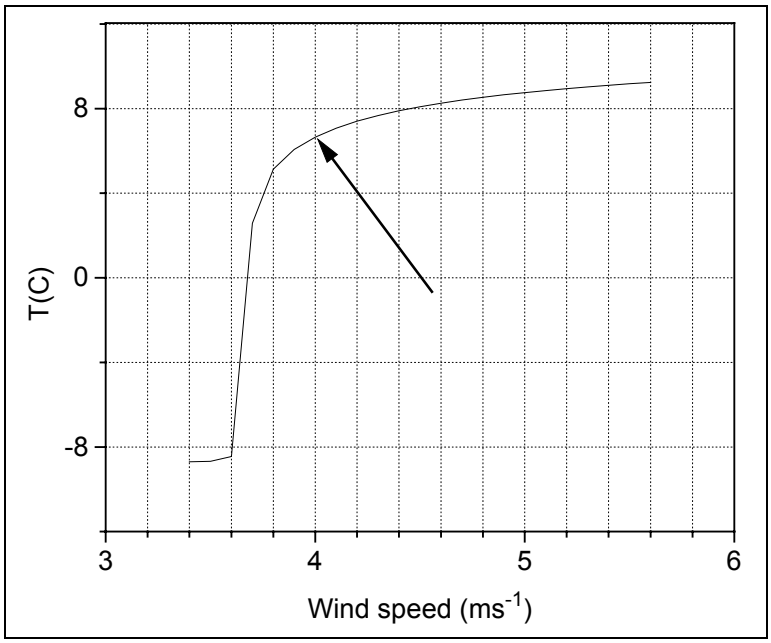

Figure 9. A more detailed view of Figure 8a.

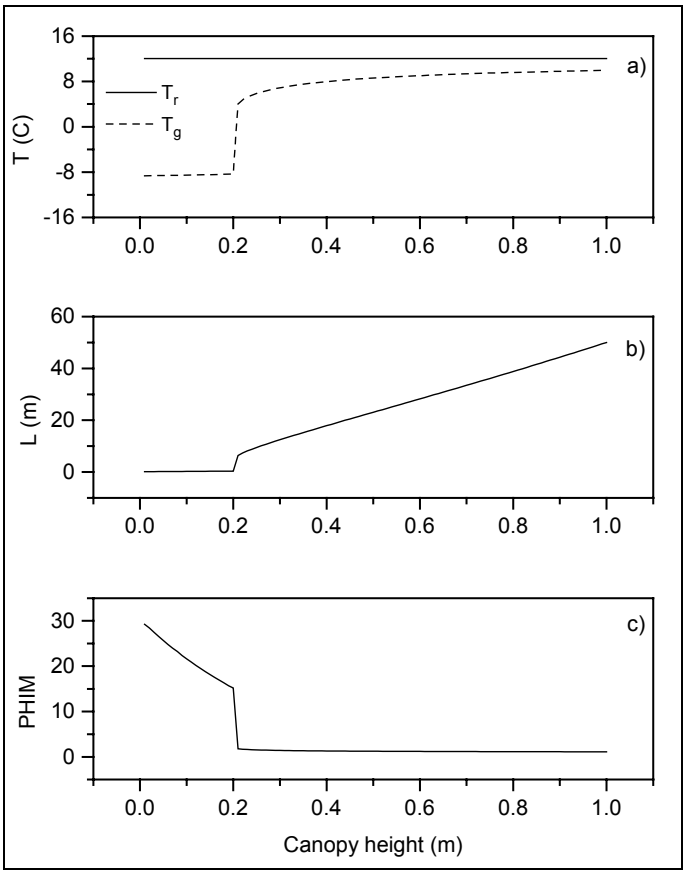

Figure 10. A plot for U_r = 3.6 ms^{-1} of a) the estimated surface temperature (T_g), b) the estimated M-O scaling length (L), and c) the estimated dimensionless wind shear (ϕ_m) as a function of the canopy height (in meters).

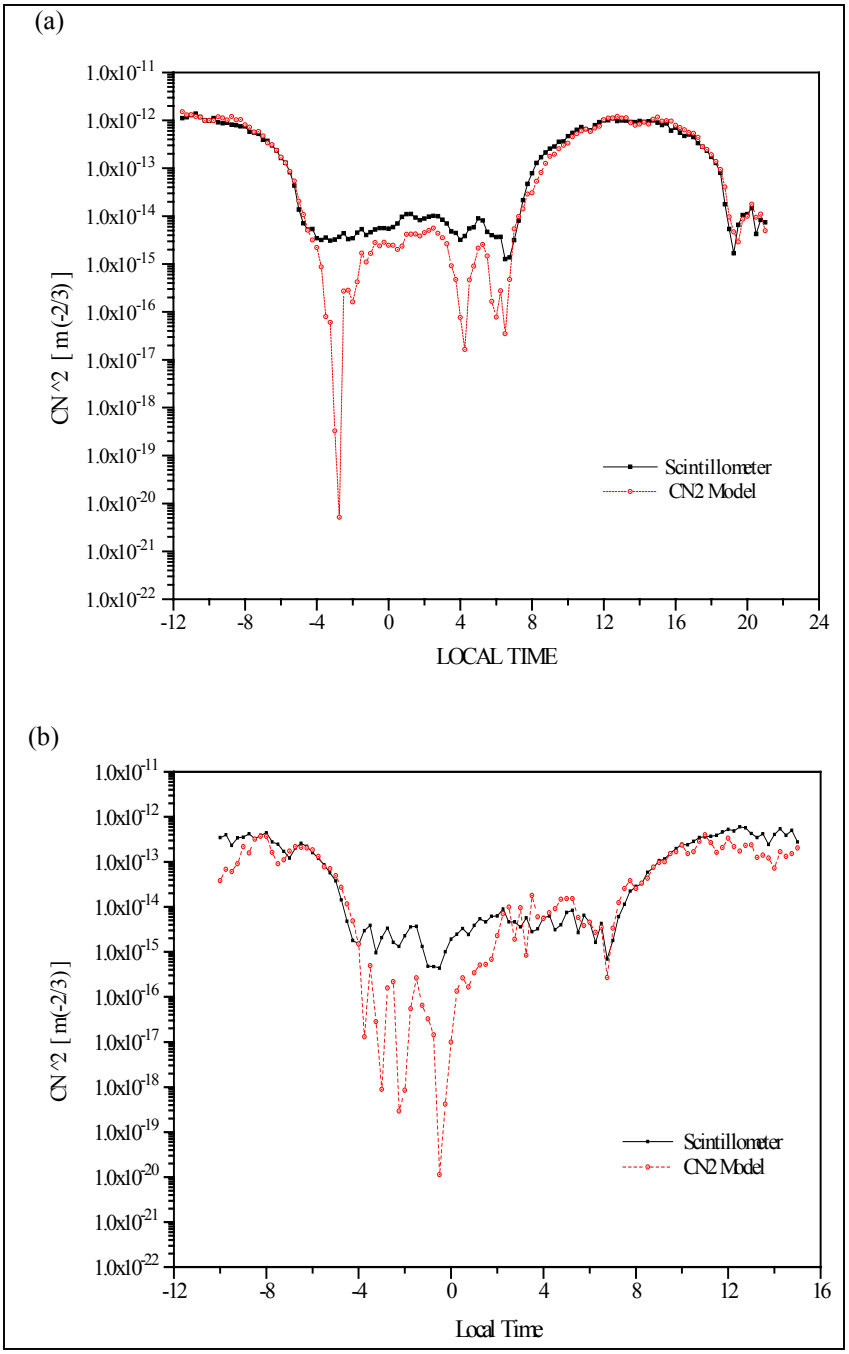

Figure 11. Time series of CN2 model output (dashed circle) compared to scintillometer data (solid square), determined from input data at 1 and 4 m above ground collected over a 450-m path on a) 8-9 July 1992 and b) 13-14 July 1992 (*42,43*).

4. Summary and Conclusions

The Army is looking to implement acoustic propagation models that will incorporate the impacts of the atmosphere, turbulence, and terrain on acoustic signatures. A key element in estimating outdoor acoustic attenuation with range (and frequency) is modeling the variation of the effective speed of sound through the lower atmosphere. M-O similarity models have been very well suited for this application, especially for daytime convective atmospheres, e.g., the energy budget and meteorological models in ABFA. However, for the nighttime case, we were interested in testing the effectiveness of an earlier quartic solution for the surface temperature, i.e., an alternate energy budget model, which explicitly computes the net surface radiation and the fluxes of heat and moisture close to the ground.

For a hypothetical nighttime case representing moderately stable atmospheric conditions, the alternate (quartic) model performed quite well. Model estimates for effective surface temperature, net radiation, sensible heat flux, soil heat flux, and latent heat flux were comparable to earlier published results (*17,18*). Also, for this case, energy budget closure was met satisfactorily. Thus, the primary energy budget model results could be used to predict profiles for wind speed, air temperature, and relative humidity, from which, effective sound speed (and ultimately acoustic attenuation) information could be generated.

However, we found that reasonable values for effective surface temperature were not obtainable from the alternate model to simulate the first nighttime IOP of the CASES-99 study. Computational difficulties were experienced because of low roughness height and low wind speed. We found that as the M-O scaling length becomes small, the energy budget model breaks down and the computation is not viable. Thus, until better solutions can be realized through future modeling or experimental works, we recommend that the alternate model be applied only when input canopy height and reference level wind speeds can affect values for the M-O scaling length larger than about *13* m.

5. References

1. Fong, M; Srour, N. *Cueing of the surrogate remote sentry using an acoustic detection system*, ARL-TR-795, U.S. Army Research Laboratory, Adelphi, MD, 1994.

2. Srour, N. "*Army acoustics needs. Sensor arrays, distributed sensors and applications*." DARPA Air-Coupled Acoustic Micro Sensors Workshop, Crystal City, VA, August 24-25. Available online from the Defense Advanced Research Projects Agency at http://www.darpa.mil/mto/sono/sensorarrays.html, 1999.

3. Srour, N.; Robertson, J. *Remote netted acoustic detection system*; ARL-TR-706, U.S. Army Research Laboratory, Adelphi, MD, 1995.

4. Wilson, D. K. Sound field computations in a stratified, moving medium. *Journal of the Acoustical Society of America* **1993**, *94*, 400–407.

5. Osteshev, V. E. Acoustics in Moving Inhomogeneous Media. *E&FN Spon Press, London*. **1997**, pp. 16, *67*, 193–218.

6. Wilson, D. K. A turbulence spectral model for sound propagation in the atmosphere that incorporates shear and buoyancy forcings. *Journal of the Acoustical Society of America* **2000**, *108*, 2021–2038.

7. Noble, J. M. User's manual for the Microsoft window edition of the scanning fast-field program (SCAFFIP) version 3.0; ARL-TR-2696; U.S. Army Research Laboratory, Adelphi, MD, 2003.

8. Wilson, D. K. Computational and Information Sciences Directorate, U.S. Army Research Laboratory, 2002.

9. Wong, G. S. K.; Embleton, T. F. W. Variation of specific heats and of specific heat ratio in air with humidity. *Journal of the Acoustical Society of America* **1984**, *76*, 555–559.

10. Monin, A. S.; Obukhov, A. M. Basic Regularity in Turbulent Mixing in the Surface Layer of the Atmosphere. *Trudy, Akademiia Nauk S.S.S.R., Geofizicheskogo Instituta* **1954**, *24*, 151.

11. Busch, N. E. On the mechanics of atmospheric turbulence. *In Workshop on Micrometeorology*. D. A. Haugen, Ed., American Meteorological Society **1973**, 392.

12. Dyer, A. J. A Review of Flux-Profile Relationships. *Boundary Layer Meteorology* **1974**, *1*, 363–372.

13. Hicks, B. B. Wind Profile Relationships from the Wangara Experiment. *Quarterly Journal of the Royal Meteorological Society* **1976**, *102*, 535–551.

14. Webb, W. K. Profile relationships: The log-linear range, and extension to strong stability. *Quarterly Journal of the Royal Meteorological Society* **1970***, 96*, 67–90.

15. Wilson, D. K. *A prototype acoustic battlefield decision aid incorporating atmospheric effects and arbitrary sensor layouts*; ARL-TR-1708; U.S. Army Research Laboratory, Adelphi, MD, 1998.

16. Wilson, D. K.; Szeto, G. L. *Reference Guide for the Acoustic Battlefield Aid (ABFA) Version 2*; ARL-TR-2159; U.S. Army Research Laboratory, Adelphi, MD, 2000.

17. Rachele, H.; Tunick, A. Energy Balance Model for Imagery and Electromagnetic Propagation. *Journal of Applied Meteorology* **1994***, 33*, 964–976.

18. Rachele, H.; Tunick, A. D.; Kordova, L.; Mahrer, Y. A radiation and energy balance model for the microscale-surface layer environment. In proceedings of the 22nd Conference on Agricultural and Forest Meteorology, Atlanta, *American Meteorological Society*, Boston, MA, **1996**.

19. Swanson, D.; Reichard, K. Environmental Sensors and Algorithms for Ground-Based Passive Acoustic Sensors. *presented at the 12th SPIE Annual International Symposium on Aerospace/Defense Sensing, Simulation and Controls*, Orlando, FL **13–17 April 1998**, *3393*, 195–206.

20. Swanson, D. C. Performance model incorporating weather related constraints for fields of unattended ground sensors. *In proceedings of Unattended Ground Sensor Technologies and Applications*. Edward M. Carapezza, David B. Law, and K. Terry Stalker (Editors), SPIE **1999**, *3713*, 197–206.

21. Stull, R. B. An Introduction to Boundary Layer Meteorology. *Kluwer Acedemic Press, Dordrecht, The Netherlands* **1988**, 666.

22. Carson, D. J. An Introduction to the Parameterization of Land-Surface Processes: Part 1. Radiation and Turbulence. *Meteorological Magazine* **1987**, *116*, 229–242.

23. Meyers, T. P; Dale, R. F. Predicting Daily Insolation With Hourly Cloud Height and Coverage. *Journal of Climate and Applied Meteorology* **1983**, *22*, 537–545.

24. Haurwitz, B. Insolation in relation to cloudiness and cloud density. *Journal of Meteorology* **1945**, *2*, 154–166.

25. Gates, D. M. Radiant Energy, Its Receipt and Disposal. *in Meteorological Monographs, Agricultural Meteorology* **1965**, *6*, 1–26.

26. Paltridge, G. W.; Platt, C. M. R. Radiative Processes in Meteorology and Climatology. *Elsevier* **1976**, 318.

27. Yamada, T. A Numerical Study of Turbulent Air Flow In and Above Forest Canopy. *Journal of the Meteorological Society of Japan*, **1981**, *60*, 439–454.

28. Rachele, H.; Tunick, A.; Hansen, F. V. MARIAH- A Similarity Based Method for Determining Wind, Temperature, and Humidity Profile Structure in the Atmospheric Surface Layer. *Journal of Applied Meteorology* **1995**, *34*, 1000–1005.

29. Mahrt, L. Stratified atmospheric boundary layers and breakdown of models. *Theoretical and Computational Fluid Dynamics*, **1998**, *11*, 263–279.

30. Högström, U. Review of some basic characteristics of the atmospheric surface layer. *Boundary Layer Meteorology*, **1996**, *78*, 215–246.

31. Rogers, R. R. A Short Course in Cloud Physics. *Second Edition, Pergamon Press, Elmsford, New York*, **1979**.

32. Rachele, H. U.S. Army Atmospheric Sciences Laboratory, White Sands Missile Range, NM, 1993.

33. Burridge, D. M.; Gadd, A. J. *The Meteorological Office Operational 10 Level Numerical Weather Prediction Model*. British Meteorological Office Technical Notes, Nos. 12 and 48, London Rd., Bracknell, Berkshire, RG12 2SZ, England, 57 pp., 1974.

34. Benoit, R. On the Integral of the Surface Layer Profile-Gradient Functions. *Journal of Applied Meteorology*, **1977**, *16*, 859–860.

35. Nickerson, E. C.; Smiley, V. E. Surface Layer and Energy Budget Parameterizations for Mesoscale Models. *Journal of Applied Meteorology*, **1975**, *14*, 297–300.

36. Campbell, G. S. and J. M. Norman. *An Introduction To Environmental Biophysics*. 2nd edition, Springer-Verlag, New York **1998**, 286.

37. Paulson C. A. The Mathematical Representation of Wind Speed and Temperature Profiles in the Unstable Atmospheric Surface Layer. *Journal of Applied Meteorology* **1970***, 9*, 857–861.

38. Noble, J. M.; Marlin, D. "*User's manual for the scanning fast field program (SCAFFIP) general version 1.0.*" ARL-TR-545; U.S. Army Research Laboratory, Adelphi, MD, 1995.

39. Poulos, G. S.; Blumen, W.; Fritts, D. C.; Lundquist, J. K.; Sun, J.; Burns, S. P.; Nappo, C.; Banta, R.; Newsom, R.; Cuxart, J.; Terradellas, E.; Balsley, B.; Jensen, M. CASES-99: A comprehensive investigation of the stable nocturnal boundary layer. *Bulletin of the American Meteorological Society*, **2002***, 83*, 555–581.

40. Mahrt, L. College of Oceanic and Atmospheric Sciences, Oregon State University, 2003.

41. Frederickson, P.A.; Davidson, K. L.; Zeisse, C. R.; Bendall, C. S. Estimating the refractive index structure parameter (C_n^2) over the ocean using bulk methods. *Journal of Applied Meteorology* **2000**, *39*, 1770–1783.

42. Tunick, A. "*The refractive index structure parameter/Atmospheric optical turbulence model:CN2*." ARL-TR-1615; U.S. Army Research Laboratory, Adelphi, MD, 1998.

43. Tunick, A. CN2 Model To Calculate The Micrometeorological Influences On The Refractive Index Structure Parameter. *Environmental Modeling and Software* **2003**, *18*, 165–171.

Distribution

Admnstr
Defns Techl Info Ctr
ATTN DTIC-OCP
8725 John J Kingman Rd Ste 0944
FT Belvoir VA 22060-6218

DARPA
ATTN S Welby
3701 N Fairfax Dr
Arlington VA 22203-1714

US Military Acdmy
Mathematical Sci Ctr of Excellence
ATTN LTC T Rugenstein
Thayer Hall Rm 226C
West Point NY 10996-1786

Sci & Technlgy Corp
10 Basil Sawyer Dr
Hampton VA 23666-1340

US Army CRREL
ATTN CECL-GP M Moran
ATTN E L Andreas
72 Lyme Rd
Hanover NJ 03755-1290

US Army Dugway Proving Ground
DPG Meteorology Div
ATTN J Bowers
West Desert Test Center
Dugway UT 84022-5000

Nav Postgraduate Schl Dept of Meteorology
ATTN P Frederickson
1 University Cir
Monterey CA 93943-5001

Air Force
ATTN Weather Techl Lib
151 Patton Ave Rm 120
Asheville NC 28801-5002

Colorado State Univ Dept of Atmos Sci
ATTN R A Pielke
200 West Lake Street
FT Collins CO 80523-1371

Duke Univ Pratt Schl of Engrg
Dept of Civil & Environ Engrg
ATTN R Avissar
Hudson Hall-Box 90287
Durham NC 27708

The City College of New York
Dept of Earth & Atmos Sci
ATTN S D Gedzelman
J106 Marshak Bldg 137th and Convent Ave
New York City NY 10031

Univ of Alabama at Huntsville
Dept of Atmos Sci
ATTN R T Mcnider
Huntsville AL 35899

Natl Ctr for Atmos Rsrch
ATTN NCAR Library Serials
PO Box 3000
Boulder CO 80307-3000

Director
US Army Rsrch Lab
ATTN AMSRL-RO-D JCI Chang
ATTN AMSRL-RO-EN W D Bach
PO Box 12211
Research Triangle Park NC 27709

US Army Rsrch Lab
ATTN AMSRL-D D R Smith
ATTN AMSRL-DD J M Miller
ATTN AMSRL-CI J D Gantt
ATTN AMSRL-CI-CS R Meyers
ATTN AMSRL-CI-EE A Tunick (12 copies)
ATTN AMSRL-CI-EE P Clark
ATTN AMSRL-CI-IS-R Mail & Records Mgmt
ATTN AMSRL-CI-IS-T Techl Pub (2 copies)
ATTN AMSRL-CI-OK-TL Techl Lib
(2 copies)
ATTN AMSRL-SE-EE Z G Sztankay
ATTN AMSRL-SE-SA N Srour
Adelphi MD 20783-1197